Received: 9 May 2019 | Revised: 23 August 2019 | Accepted: 9 September 2019

DOI: 10.1111/cmi.13122

RESEARCH ARTICLE

WILEY

Illuminating the dark depths inside coral

Chichi Liu[1] | Shuk Han Cheng[2] | Senjie Lin[1,3]

[1] State Key Laboratory of Marine Environmental Science, College of Ocean and Earth Sciences, Xiamen University, Xiamen, China

[2] Department of Biomedical Sciences, City University of Hong Kong, Hong Kong, China

[3] Department of Marine Sciences, University of Connecticut, Groton, Connecticut

Correspondence
Senjie Lin, Department of Marine Sciences, University of Connecticut, Groton, CT 06340, USA.
Email: senjie.lin@uconn.edu

Shuk Han Cheng, Department of Biomedical Sciences, College of Veterinary Medicine and Life Science, City University of Hong Kong, Hong Kong 999077, China.
Email: bhcheng@cityu.edu.hk

Funding information
China Postdoctoral Fund, Grant/Award Number: 2017M620271; Projects of International Cooperation and Exchanges, Grant/Award Number: NSFC 31661143029; Collaborative Research Fund, Grant/Award Number: 8730037; National Key Research and Development Program of China (973 program), Grant/Award Numbers: 2016YFA0601202 and 2017YFC1404302

Abstract

The ability to observe in situ 3D distribution and dynamics of endosymbionts in corals is crucial for gaining a mechanistic understanding of coral bleaching and reef degradation. Here, we report the development of a tissue clearing (TC) coupled with light sheet fluorescence microscopy (LSFM) method for 3D imaging of the coral holobiont at single-cell resolution. The initial applications have demonstrated the ability of this technique to provide high spatial resolution quantitative information of endosymbiont abundance and distribution within corals. With specific fluorescent probes or assays, TC-LSFM also revealed spatial distribution and dynamics of physiological conditions (such as cell proliferation, apoptosis, and hypoxia response) in both corals and their endosymbionts. This tool is highly promising for in situ and in-depth data acquisition to illuminate coral symbiosis and health conditions in the changing marine environment, providing fundamental information for coral reef conservation and restoration.

KEYWORDS

3D imaging, cellular hypoxia, coral, light sheet fluorescence microscopy, Symbiodiniaceae, tissue clearing

1 | INTRODUCTION

Coral reefs, the most species-rich and productive ecosystem in the ocean, are threatened by accelerated global climate and environmental changes (Hoegh-Guldberg et al., 2007; Hughes et al., 2003; Hughes et al., 2017; Hughes et al., 2017; Hughes et al., 2018; Hughes et al., 2018). Damages are mostly rooted in the disruption of the symbiosis between hermatypic corals and their endosymbionts, which are algae belonging to the dinoflagellate family Symbiodiniaceae (Hoegh-Guldberg, 1999; LaJeunesse et al., 2018; Rowan & Knowlton, 1995). Coral beaching, a major cause of coral degradation, occurs as the coral host expels the endosymbionts and hence loses the characteristic pigment of the algae in response to environmental stress (van Oppen & Lough, 2008; Weis, 2008). To understand how environmental stress causes coral bleaching and why different species of Symbiodiniaceae respond differently to stress, researchers have performed extensive studies from molecular, cellular, to ecosystem levels (Davy, Allemand, & Weis, 2012; De'ath, Fabricius, Sweatman, & Puotinen, 2012; Nielsen, Petrou, & Gates, 2018; Putnam, Barott, Ainsworth, & Gates, 2017; Stat, Morris, & Gates, 2008; Weis, 2008). Live observation of corals and documentation of their behaviour or physiology have also been carried out through underwater microscopy (Mullen et al., 2016) and coral-on-a-chip approach (Shapiro, Kramarsky-Winter, Gavish, Stocker, & Vardi, 2016). However, spatial organisation of the endosymbionts and spatially resolved physiological dynamics of the holobiont in the process of stress response and stress-induced dysbiosis are largely intractable due to the lack of proper techniques that allow in-depth observations in toto.

Here, leveraging the power of light sheet fluorescent microscopy (LSFM) and tissue clearing (TC) technology, we developed a whole mount 3D imaging method to directly observe symbiont organisation and coral/symbiont physiologies *in toto*. LSFM features a fast acquisition speed, a low phototoxicity, and a high efficiency for imaging thick biological samples (Huisken & Stainier, 2009; Huisken, Swoger, Del

Bene, Wittbrodt, & Stelzer, 2004; Power & Huisken, 2017; Reynaud, Peychl, Huisken, & Tomancak, 2015). It alone is promising for imaging fixed (Capoulade, Reynaud, & Wachsmuth, 2013) and live (Laissue, Alghamdi, Tomancak, Reynaud, & Shroff, 2017) coral samples, but the resolution and imaging depth are compromised by the blockage of illumination by coral skeleton and the low transparency of coral tissues. TC, a frequently employed tool in biomedical research (Azaripour et al., 2016; Chung et al., 2013; Dodt et al., 2007; Richardson & Lichtman, 2015), has the potential to address this issue. In this study, we developed a protocol combining LSFM and TC. In the initial limited-scope application of this method, we successfully obtained 3D see-through images of coral tissue and demonstrated a broad range of utility in studying physiologies and stress responses of coral hosts and their endosymbionts.

2 | EXPERIMENTAL PROCEDURES

2.1 | Coral sample collection and maintenance

Healthy *Seriatopora hystrix* and *Seriatopora* sp. were acquired from a coral aquarium tank. Bleached *S. hystrix* and *Seriatopora stellate* were collected by scuba diving in Bohol, Philippines in October 2017 (only 1 cm of branch tip was sampled). Similarly, bleached *Acropora* sp. were collected by scuba diving in Hong Kong. Coral samples were fixed in 4% paraformaldehyde (PFA) prepared in 0.45-μm filtered seawater (FSW) immediately after collection and processed in the laboratory.

2.2 | TC of coral sample

The fixed coral fragments were washed with 0.01-M Phosphate-Buffered Saline (PBS) thrice at room temperature with gentle shaking. Coral skeleton was removed through decalcification conducted in 10% ethylenediaminetetraacetic acid at pH 7.4. The solution was replaced twice every day until the whole skeleton was removed. Methanol was used for decolorising and permeabilisation. The samples were washed with PBS thrice and dehydrated in 50%, 75%, 90%, and 100% methanol in 0.01-M PBS for 10 min at each step with gentle shaking. The samples were then rehydrated in 90%, 75%, and 50% methanol in 0.01-M PBS containing 0.2% Triton X-100 (PBST) for 10 min at each step with gentle shaking. Incubation time was carefully controlled to preserve the autofluorescence signal of chlorophyll during LSFM imaging. The samples were washed with PBST thrice and fluorescence labelled in accordance with the detailed procedure as described below. The samples for measuring the density of Symbiodiniaceae were only directly subjected to refractive index (RI) matching step. RI matching was performed by immersing the sample in an RI matching solution (RIMS, Yang et al., 2014), which was obtained by dissolving 20 g of Nycodenz (Axis-Shield Diagnostics) in 16 ml of 0.02-M PBS and adjusting RI to 1.45 by using water. After 2 to 4 hr of immersion, RIMS was renewed to maintain the RI value. 4′,6-diamidino-2-phenylindole (DAPI) was added to RIMS in the second round of immersion with the final concentration of 1 μg/ml to improve the staining of the coral tissue. After 1 to 2 hr of immersion and staining, the cleared coral sample was ready for LSFM imaging as described below.

2.3 | Micropropagation of *Pocillopora damicornis*

Coral micropropagates were obtained through a polyp bailout assay. *P. damicornis* fragments were placed in a Petri dish filled with FSW, and the salinity of which was gradually adjusted to 50 PSU within 5 hr by using high-salinity FSW (60 PSU). The bailout polyps were examined under a stereomicroscope. Some of the micropropagates were fixed immediately with 4% paraformaldehyde prepared in FSW. These samples were used as newly separated polyps for apoptotic cell detection via a terminal deoxynucleotidyl transferase dUTP nick end labeling (TUNEL) assay. Some of the micropropagates were gradually transferred to normal salinity at 33–35 PSU and frequently examined under a stereomicroscope. Once the micropropagates flattened, which indicated the initiation of reattachment, the samples were fixed as previously described. These samples were used as newly reattached coral micropropagates for cell mitosis detection through immunofluorescence assay.

2.4 | Cell proliferation and apoptosis detection

Fluorescence labelling of proliferating cells were achieved by using an EdU cell proliferation assay kit (C10638, Thermo Fisher Scientific, US). A coral fragment was placed in a sealed chamber filled with 50–100 times volume of FSW containing 20-μM EdU. The chamber was incubated in a coral aquarium tank to maintain an optimal temperature of 26°C and a light intensity of approximately 100 $\mu E \cdot m^{2} \cdot s^{-1}$. After 1 hr of incubation, the coral branch was cut into small pieces by using a bone cutter, fixed in 4% paraformaldehyde prepared in FSW, decalcified, and decolorised as previously described. EdU was detected in accordance with the manufacturer's instructions with slight modifications. In general, the volumes of the reagents used in the assay were adjusted to about 20–30 times the volume of the coral samples, and they were incubated two times longer to achieve the whole tissue detection of the incorporated EdU. The samples were then subjected to DAPI staining and RI matching as previously described. Light exposure was avoided.

TUNEL assay (G3250, Promega, US) was used for fluorescence labelling of apoptotic cells. Sample fixation, decalcification, and decolorisation were conducted as described above. The samples were permeabilised with 20–30 times the volume of 20-μg/ml Proteinase K at room temperature for 30 min, washed with 0.01-M PBS thrice, and equilibrated at room temperature for 20 min with 20 times the volume of terminal deoxynucleotidyl transferase (TdT) buffer. A TdT reaction was carried out with 20 times the volume of a TdT reaction mix (containing TdT buffer, fluorescence labelled nucleotide mix, and rTdT enzyme) at 37°C for 90 min. TdT enzyme negative control was conducted simultaneously. After the TdT reaction, the samples were subjected to DAPI staining and RI matching as described above.

2.5 | Whole mount immunofluorescence of histone H3 phosphorylation in coral tissues

For immunofluorescence staining, sample fixation, decalcification, and decolorisation were conducted as described earlier. Blocking was performed using blocking buffer (PBST containing 2% BSA and 2% goat serum) at room temperature for 2 to 4 hr. Primary antibody (rabbit anti-histone H3 [Ser10]; EMD Millipore, USA) was diluted (1:500) in blocking buffer and incubated with the coral tissues at 4°C overnight. The coral sample was then washed with PBST thrice for 30 min at each step and incubated with Alexa Fluor 488-conjugated goat anti-rabbit IgG (A11034, Invitrogen, 1:200, Invitrogen) as a secondary antibody at 4°C overnight. The samples were washed thrice with PBST for 30 min at each step and subjected to DAPI staining and RI matching as described above.

2.6 | Detection of cellular hypoxia of coral tissues

A coral nubbin was placed in a sealed respiration chamber filled with FSW in the dark to induce coral tissue hypoxia. After 5 hr of incubation, pimonidazole hydrochloride (Hypoxyprobe-Red549 Kits, Hypoxyprobe, USA) was added with a final concentration of 300 nM. After 1 hr of incubation, coral nubbins were then fixed with 4% PFA in FSW for 2 hr at room temperature or overnight at 4°C. The whole process was conducted under low light to avoid changes in cellular oxygen concentrations due to photosynthesis. The samples were then decalcified and decolorised as described earlier. Dylight549 conjugated antibody (1:50 dilution) was utilised to detect the intracellular content of a pimonidazole adduct. The subsequent procedure was similar to the whole mount immunofluorescence protocol described above. The coral samples that were not subjected to hypoxyprobe incubation were used as negative control, whereas the coral samples incubated in the dark with air bubbles were set as normoxic control. The samples were finally subjected to DAPI staining and RI matching as described earlier.

2.7 | Coral sample mounting and light sheet imaging

3D images of the coral samples were taken using ZEISS lightsheet Z.1 system. The samples were mounted in accordance with the guidelines provided by ZEISS with some modifications. A glass capillary from ZEISS with an inner diameter of 2 mm, a 1-ml syringe with an inner diameter of 4.7 mm, and a glass tube with inner diameters of 3.5 and 6 mm with a custom-made plunger were used to mount the coral samples with an appropriate size. A 3D-printed adaptor was used to fasten the glass tube to the syringe sample holder of the microscope (Figure S2). After RI was adjusted, the coral samples were transferred to a mounting medium (RIMS with 1.5% low-melt agarose, RI = 1.450, 50°C to 55°C), gently inverted several times to avoid bubble formation, and incubated for 5 min. The sample was then loaded to the mounting tube with an appropriate inner diameter and placed at 4°C in a light-proof moisture chamber for at least 1 hr to allow the solidification of the mounting medium. The samples were mounted and immediately imaged or stored at 4°C in the moisture chamber until they were subsequently imaged. Before imaging was performed, the samples stored for hours or longer were re-immersed in RIMS to re-adjust RI to 1.45.

A clearing (RI = 1.45) optical setting with a 5× objective was applied to the ZEISS lightsheet Z.1 system, whereas a 0.6–1.5× tube lens was used depending on the size of the coral sample. Under this condition, z-stepping was 2 or 2.5 μm with 4- or 5-μm thickness of a laser sheet. In this setting, 500 or 400 optical sections for 1-mm thick coral tissues were produced, thereby allowing the precise 3D reconstruction of the coral sample. The imaging chamber was filled with RIMS (RI = 1.45) and frequently monitored using a refractometer (NAR-1 T, ATAGO, US). The cylinder of the solidified mounting medium containing the coral sample was pushed out from the glass capillary or the syringe, equilibrated for 10 to 20 min, and imaged. The coral samples with a thickness of >600 μm were subjected to two-view image acquisition and post-imaging fusion. DAPI was excited using a 410-nm laser, and the fluorescence signal was collected with a 490-nm bandpass filter. Coral green fluorescence protein and apoptosis TUNEL assays were excited using a 488-nm laser and collected with a 533-nm bandpass filter. Dylight549, Alexa Fluor 555, and CY3 were excited using a 561-nm laser and collected with a 590-nm bandpass filter. The autofluorescence of the chlorophyll was excited using a 410-nm laser and collected with a 610-nm long-pass emission filter. The samples in one experiment were captured under identical conditions of laser power, exposure time, laser sheet thickness, and z-stepping.

2.8 | Quantitative analysis of 3D image data

Multiview image data were fused and deconvoluted with ZEN software (Black edition, ZEISS). Identical gamma value and dynamic range were applied to all of the samples to obtain consistent results. Afterward, 3D reconstruction was performed using arivis Vision4D (Version 2.12.4). The volume of the chlorophyll autofluorescence signal of Symbiodiniaceae cells was calculated using an analysis pipeline of the intensity threshold and followed by a segment filter in Vision4D. All of the signals were sorted in the order of volume first, and the roundness of x-y projection and the sphericity of the sorted fluorescence signal were plotted in the same order. The drop of roundness and sphericity indicated that the signal contained two or more Symbiodiniaceae cells that were too close to be separated (Figure 3c, d). Based on the signal volume value (not intensity value) and information on roundness and sphericity, single-cell signals were identified. The average volume of the signal from a single Symbiodiniaceae cell was then calculated from the single-cell signals. The total number of Symbiodiniaceae cells was then obtained by dividing the total signal volume with the average single-cell signal. The average diameter of Symbiodiniaceae cells was calculated from the area of the x-y projection of the single Symbiodiniaceae signal. Red, green, and blue (RGB) threshold filter followed by a volume segment filter was used for identifying mitotic Symbiodiniaceae cells, which has chlorophyll red fluorescence and green fluorescence. The number of signals of the other

physiological parameters, such as cell proliferation and cell apoptosis, were counted directly by using a similar analysis pipeline with a proper threshold setting.

DAPI signal was used to calculate the volume and surface area of the coral samples. Serial longitudinal optical sections were converted to cross-sections by using the series modify function of ZEN software and then fed to Vision4D for 3D reconstruction to calculate volume. The intensity threshold and the segment filter were used as an analysis pipeline; proper threshold settings were applied to different samples in one experiment. The surface areas of the branch coral samples were estimated as the area of the equivalent unfolded cylinder based on sample height and volume. The scope of analysis was adjusted in three dimensions to calculate the number of Symbiodiniaceae cells and the volume of the tissues in a specific area.

3 | RESULTS

3.1 | See-through 3D imaging of the coral samples

The coral samples were fixed on site by using paraformaldehyde to preserve under in situ conditions. Decolorisation was conducted to the samples while the fluorescent signal of the chlorophyll was still detectable to easily distinguish Symbiodiniaceae from the coral tissue and to minimise light absorption. The transparency of the coral sample immersed in an aqueous TC solution with an RI of 1.45 was significantly enhanced (Figure 1a). Target-specific information could be obtained through bioimage informatics analysis by collecting the in toto fluorescence signal of the tissue-cleared coral sample through LSFM. As an example of our initial applications of the technique, the

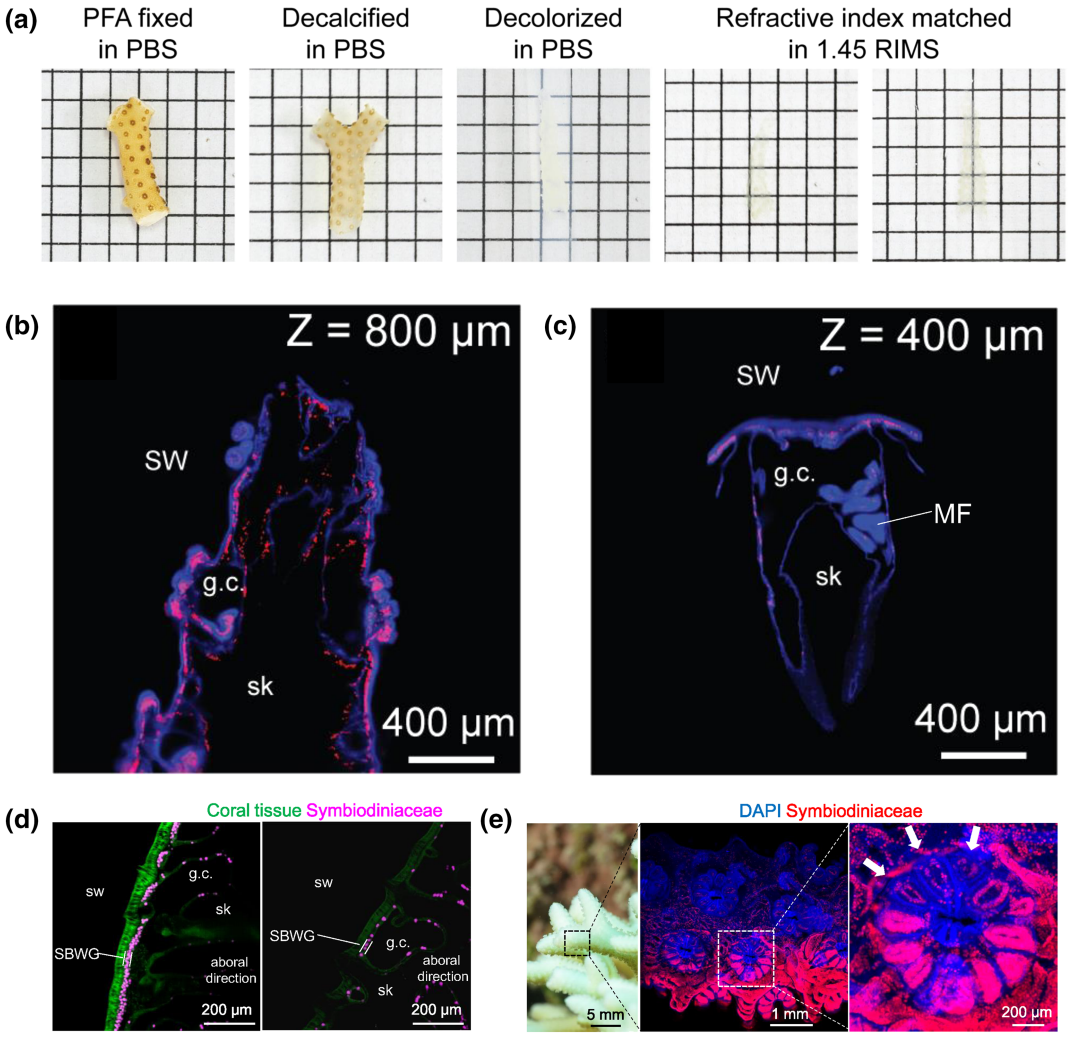

FIGURE 1 Tissue clearing and light sheet imaging of the coral sample. (a) Brightfield images demonstrating the transparency of the coral samples after each step of the treatment. (b) Image illustrating 1 out of 857 optical sections of branch tip imaging (z = 800 µm; for more data, see Figure S1a and Movie S1). (c) Image showing 1 out of 635 optical sections of the one isolated polyp of *Seriatopora* sp. (z = 400 µm; for more data, see Figure S1b). (d) Optical section of unbleached (left panel) and bleached (right panel) *Acropora* sp. (coenosarc). Green indicates the fluorescence of the green fluorescence protein in the coral tissue. (e) Close-up image of coral *S. stellate* with light-induced bleaching on the upper surface (left panel) and maximum intensity projection after FLSM-TC imaging (middle panel). Increased magnification view (right panel) shows tentacles with low Symbiodiniaceae density (white arrow) compared with the other tentacles in one polyp. g.c., gastric cavity; MF, mesenterial filaments; SBWG, surface body wall gastrodermis; sk, decalcified skeleton; SW, seawater

serial optical sections of a branch tip of *S. hystrix* were collected, and each section showed a clear fluorescence image at a certain depth of the sample (Figure 1b, Figure S1a, and Movie S1). The single polyps of *Seriatopora* sp. were successfully separated from the decalcified tissue and imaged, and optical sections deep in the tissues were acquired to clearly show the structure of the gastric cavity and the organs inside, such as the mesenterial filament (Figure 1c and Figure S1b). With these methods, the coral tissues could be clearly visualised through the blue fluorescence of the DNA-DAPI stain and the populated and heterogeneously distributed Symbiodiniaceae through the overwhelming red autofluorescence of chlorophyll.

The TC-LSFM imaging of the healthy and bleached *Acropora* sp. samples revealed that the Symbiodiniaceae density in coenosarc decreased in the surface body wall gastrodermis but not in the aboral tissue (Figure 1d). With the high spatial resolution of the technique, localised bleaching, such as that induced by excess light on the upper side of a *S. stellate* branch, could be examined and different Symbiodiniaceae densities between tentacles of one coral polyp could be documented (Figure 1e). The 3D reconstruction from the numerous optical sections yielded the high accuracy and fine spatial resolution of Symbiodiniaceae distribution in the 3D space within the coral branch tips and within the single polyps (Figure 2; Movies S2 and S3).

3.2 | Quantitative analysis of Symbiodiniaceae 3D distribution

The fluorescent signals of Symbiodiniaceae were easily identified in the 3D-rendered volumetric image of a coral sample. However, the direct counting of discrete signals would seriously underestimate the number of Symbiodiniaceae cells because multiple Symbiodiniaceae cells might be counted as one when they were too close to one another to be separated (e.g., polyp tentacles). An image informatics workflow was developed to address the challenge based on the concept of the signal volume (Figure 3). In some areas of the coral sample, the boundary of the cell signals could be easily identified because the cells existed singly or were well separated. In most parts of the coral sample, the boundary was unidentifiable (Figure 3b). In such a sample, the 2D projections of the signals from single cells (small signal

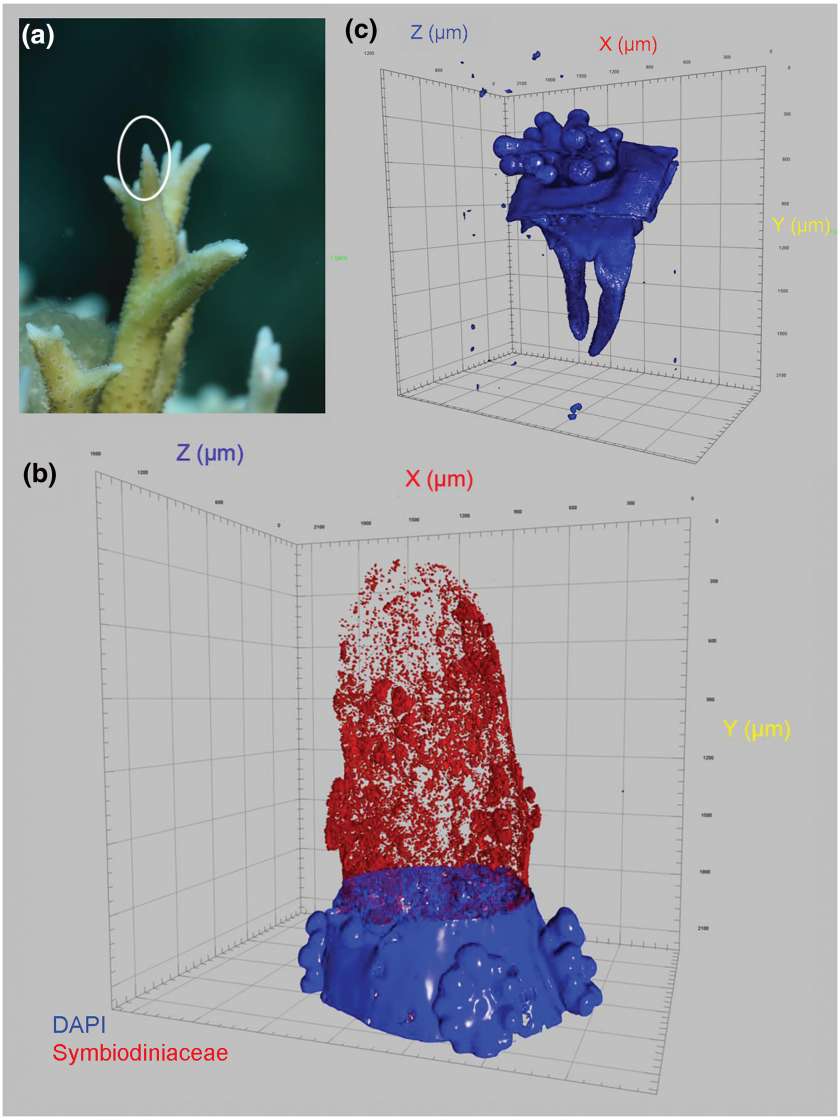

FIGURE 2 3D reconstruction of the coral sample based on serial optical sections. (a) Close-up image of coral *S. hystrix* with a branch tip (circled) to be imaged. (b) 3D reconstruction of the *S. hystrix* branch tip showing the distribution pattern of Symbiodiniaceae recognisable from its red autofluorescence of chlorophyll (shown in the upper part of the image and obtained when the coral tissue was digitally removed to create a see-through effect; blue fluorescence of the lower part is from DNA-DAPI stain of the unremoved coral tissue). For more data, see Movie S2. (c) 3D reconstruction of a *Seriatopora* sp. polyp (for more data, see Movie S3). DAPI, 4′,6-diamidino-2-phenylindole

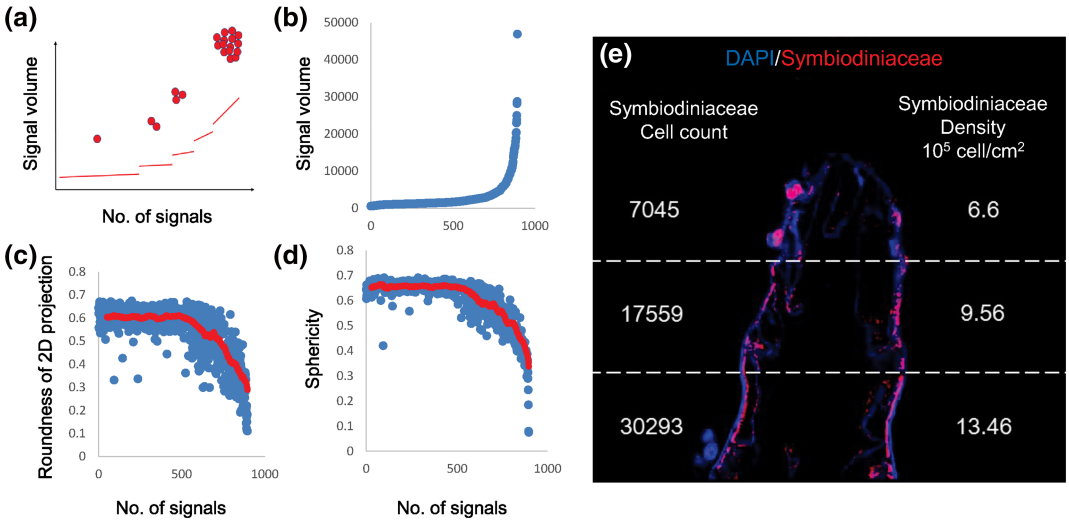

FIGURE 3 Quantification of Symbiodiniaceae density based on 3D image data by using the signal volume algorithm. (a) Concept of the signal volume calculation of a single Symbiodiniaceae cell. Filled circles represent a single cell or groups of cells. Lines depict signal volumes corresponding to the number of signals represented by the number of cells (filled circles). (b) Volumes of the identified Symbiodiniaceae signals in a coral sample increased sharply as Symbiodiniaceae cells clumped together. (c) Roundness of the 2D projection of the Symbiodiniaceae signal, which dropped precipitously when some Symbiodiniaceae cells clumped together and the signal volume exceeded a certain level. (d) Sphericity of the rendered 3D Symbiodiniaceae fluorescence signal, which declined precipitously when some Symbiodiniaceae cells clumped together and the signal volume exceeded a certain level. (e) Quantification of the number and density (cells/cm^2) of Symbiodiniaceae cells in the *S. hystrix* branch tip in Figure 1b as estimated using the signal volume algorithm by dividing the total signal volume with the single-cell signal volume. Single-cell signal was identified with the aid of the roundness and sphericity information. In all of the images, blue indicates the fluorescence of DNA-DAPI stain, whereas red denotes the autofluorescence of chlorophyll in Symbiodiniaceae cells. DAPI, 4′,6-diamidino-2-phenylindole

volumes) were perfectly round, whereas the 2D projections of the signals from two or more clumped Symbiodiniaceae cells (signal volume exceeding a certain value) showed a rapidly decreased roundness (Figure 3c). The identified clump of the multiple cells could be confirmed by the same trend of the sphericity of the 3D-rendered fluorescence signals (Figure 3d). Thus, with the help of the roundness and sphericity information, the signals of the single cells could be accurately identified. The Symbiodiniaceae cell count in a cell clump could be obtained by dividing the total Symbiodiniaceae fluorescence signal volume with the single-cell signal volume on the basis of the average signal volume of a single Symbiodiniaceae cell. The volume or surface area of the coral sample required for cell density estimation could be calculated from rendered volumetric image. Although DAPI stains DNA only in the nuclei, the fluorescence signal tended to cover the entire tissue surface of the coral sample because of the high cell density in the coral epidermis and could hence be used to reconstruct the coral tissue surface area. In the branch tip shown as an example (Figure 1b), our calculation revealed that the Symbiodiniaceae density of *S. hystrix* ranged from 6.6 × 10^5 cells cm^{-2} at the tip to 13.5 × 10^5 cells cm^{-2} towards the base (Figure 3e). The conventional method would only generate an average Symbiodiniaceae density (~10^6 cells cm^{-2} assuming 100% cell recovery) for the whole branch segment.

3.3 | 3D imaging of the coral physiology

TC-LSFM could also be performed to visualise the physiological conditions in the coral tissues. Using EdU cell proliferation assay, we imaged the numbers and spatial patterns of proliferating cells in a coral branch tip, showing a high density of proliferating cells and a low density of Symbiodiniaceae cells in the apex (Figure 4a). We obtained *P. damicornis* micropropagates through a "bailout" procedure and conducted a TUNEL assay to detect apoptotic cells during bailout and reattachment. Numerous apoptotic cells were observed, suggesting that tissue remodelling occurred immediately after the polyp bailed out (Figure 4b). We also performed the whole mount fluorescence immunolabelling of histone phosphorylation, which is a specific marker of mitosis, in newly reattached coral micropropagates (Figure 4c). Although the coral and the Symbiodiniaceae cells were labelled at the same time, the signal was distinguishable by using a segment filter because of their different volumes and red fluorescence signals from chlorophyll in Symbiodiniaceae. Quantitative results showed that mitosis was quickly initiated after re-attachment in the coral polyp (MI = 3.8%) but not in the unattached polyp (data not shown). The mitotic status of the labelled Symbiodiniaceae cells was also evidenced by their increased cell size (data not shown). The 3D reconstruction also showed that flattening of the polyp after re-attachment and the distribution of Symbiodiniaceae (Movie S4).

3.4 | Detection of cellular hypoxia in coral holobionts

Coral cells can experience hypoxia and severe stress at night due to the on and off dynamics of photosynthetic oxygen production (Zoccola et al., 2017). To address the challenge in detecting cellular hypoxia in a coral holobiont, we applied a hypoxyprobe, which is widely used in biomedical and clinical science. A pimonidazole-based hypoxyprobe easily diffuses into cells and forms adducts when the intracellular oxygen level

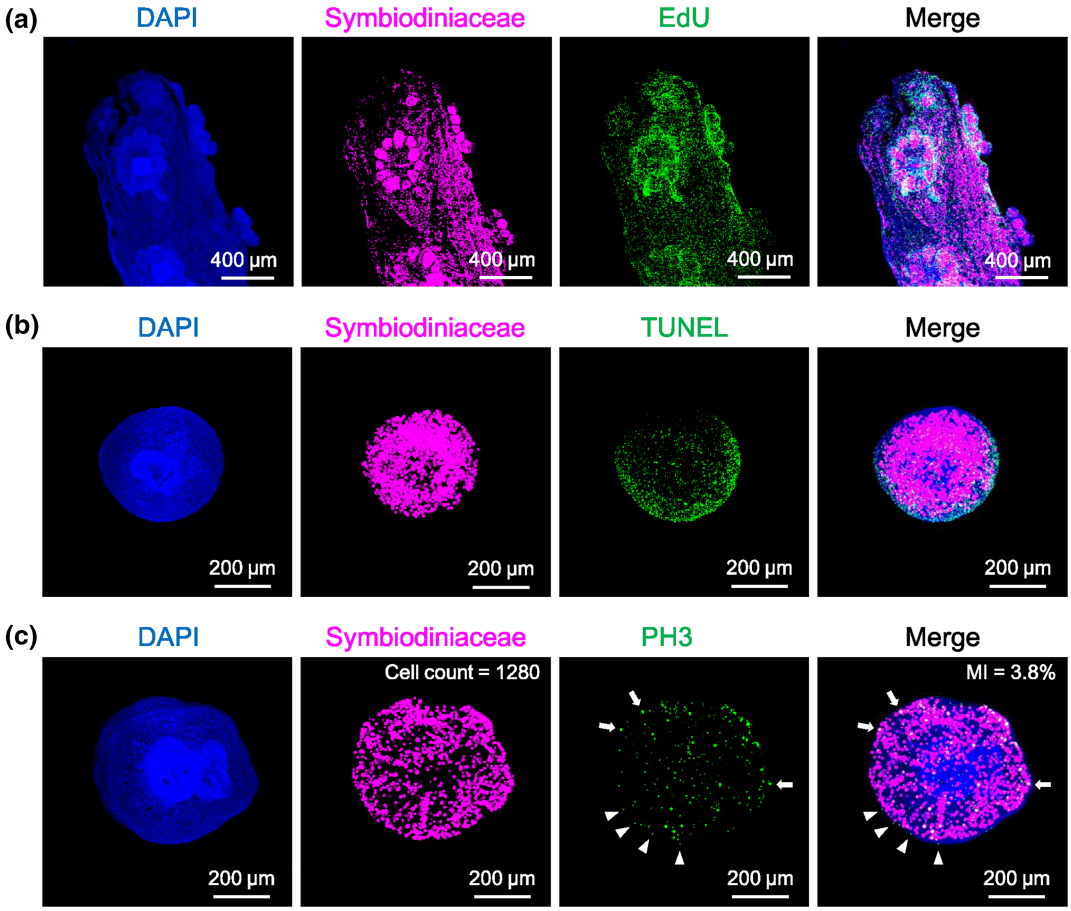

FIGURE 4 TC-LSFM coupled with various fluorescence labeling assays to probe the physiologies of coral Symbiodiniaceae systems. (a) Maximum intensity projection of *Seriatopora* sp. branch tip showing the proliferating cells detected by using EdU cell proliferation assay (green fluorescence). (b) Maximum intensity projection of apoptotic cells detected by using TUNEL assay (green fluorescence) in the bailout polyp of *Pocillopora damicornis*. (c) Immunolabelling of mitotic coral cells (arrowheads) and Symbiodiniaceae cells (arrows) detected using the histone H3 phosphorylation-specific antibody (green fluorescence) in the reattached bailout polyp of *P. damicornis* (for 3D reconstruction of the reattached polyp, see Movie S4). In all images, blue indicates the fluorescence of DNA-DAPI stain, whereas magenta denotes the autofluorescence of chlorophyll in Symbiodiniaceae cells. DAPI, 4′,6-diamidino-2-phenylindole; MI, mitotic index

decreases below 10 mmHg and allows post-fixation detection through immunofluorescence. Our results showed that the cellular hypoxia of the coral and the Symbiodiniaceae cells could be detected using TC-LSFM method (Figure 5). In this experiment, coral cell hypoxia occurred in the aboral tissue but not in the surface body wall under the dark condition without an oxygen supply (Figure 5a). A gradient of hypoxyprobe signals (green fluorescence) was observed along the tissue depth (Figure 5c). No fluorescence signal was detected in the pimonidazole negative control (Figure 5b), whereas only a weak signal was detected in the tentacle area of the normoxic control (dark condition with oxygen supply; Figure 5c). Some of the Symbiodiniaceae cells that were spatially unevenly distributed showed signs of cellular hypoxia (Figure 5d). The percentage of the hypoxia-stressed Symbiodiniaceae cells could be estimated using the signal volume algorithm described above. In the two selected areas shown in Figure 5b, similar Symbiodiniaceae densities were observed (1.81×10^5 and 2.07×10^5 for left and right panels, respectively). The percentage of the hypoxia-stressed Symbiodiniaceae cells differed significantly, from 0.5% (1 out of 196 cells) for the left panel to 44.3% (121 out of 273 cells) for the right panel.

4 | DISCUSSION

Here, we report the development of a technique by combining the existing TC technique and light sheet fluorescence microscopy. By applying this technique to a range of coral conditions, along with various probes, we also demonstrate that this new technique is powerful for collecting quantitative information on the 3D spatial distribution of Symbiodiniaceae and for elucidating the physiological conditions deep inside the corals with single-cell resolution. The heterogeneous Symbiodiniaceae distribution documented here reveals the superiority of the technique to conventional Symbiodiniaceae density measurement methods that typically give average symbiont density. Furthermore, the abundance of Symbiodiniaceae cells in total or in any part of the coral sample, per coral surface area, or per tissue volume could be easily calculated by obtaining the average fluorescence volume per Symbiodiniaceae cell and the total fluorescence volume. Even though the setting of intensity threshold during segmentation is case by case and can be subjective, the calculation would be unaffected because calculation was based on the volume of fluorescent cells rather than

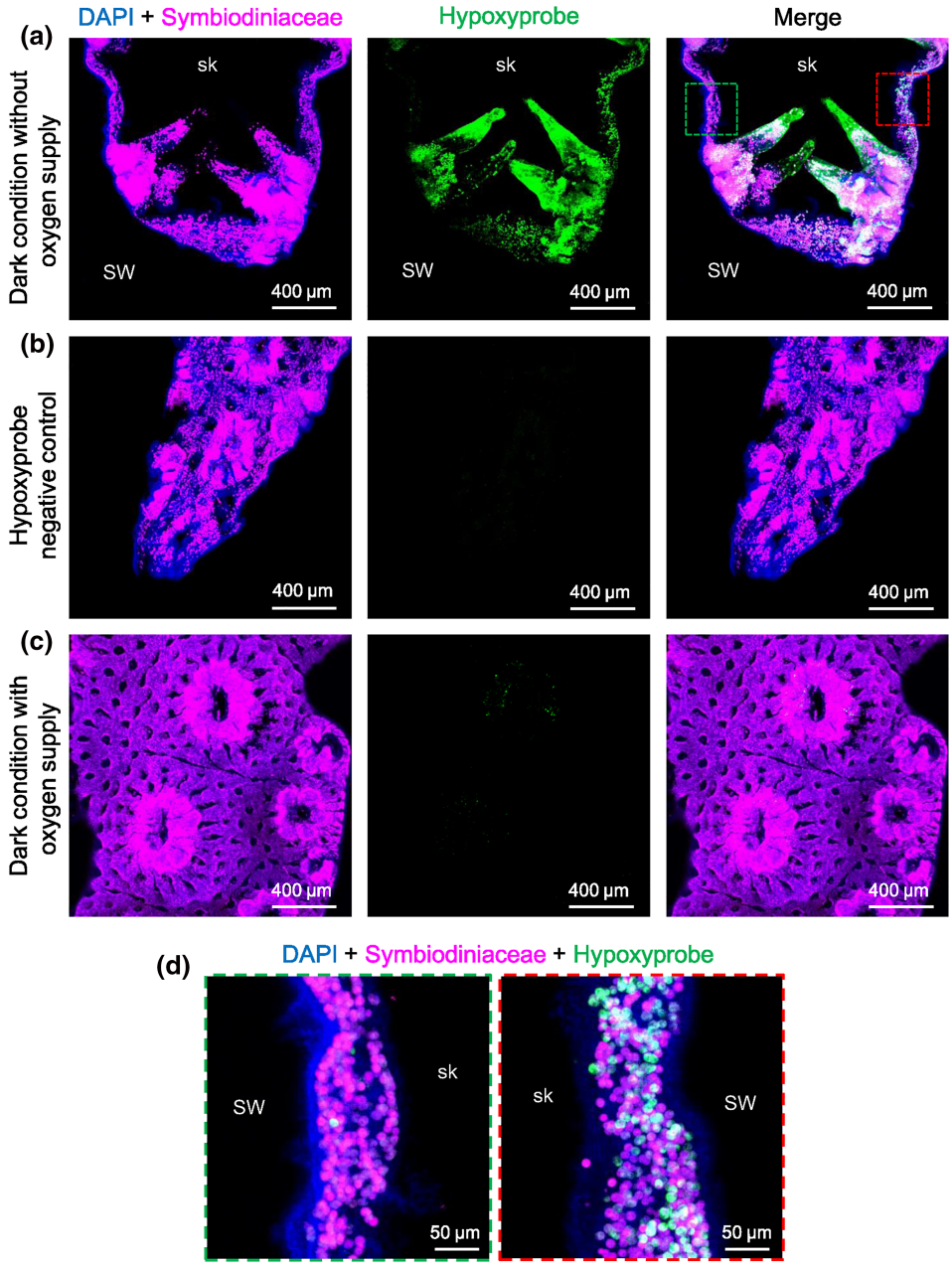

FIGURE 5 Detection of cellular hypoxia in coral holobionts by using pimonidazole-based hypoxyprobe and TCLSFM. Maximum intensity projection of hypoxia treatment (dark condition without oxygen supply) (a, crosssection), hypoxyprobe negative control (b, lateral view), and the normoxic control (dark condition with oxygen supply) (c, lateral view), showing immunofluorescence labeling of intracellular pimonidazole (green fluorescence). Magenta depicts the autofluorescence of chlorophyll in Symbiodiniaceae. Blue denotes the DNA-DAPI stain. All of the images were obtained under identical conditions and the same dynamic range and presented as the maximum intensity projection. (d) Increased magnification view of the area marked by the corresponding coloured rectangle in the right panel of (a), showing the localised distribution of hypoxic Symbiodiniaceae cells in the surface body wall gastrodermis. DAPI, 4′,6-diamidino-2-phenylindole; sk, decalcified skeleton; SW, seawater

the intensity of fluorescence. For example, lower intensity threshold gives larger total signal volume, but it gives bigger single-cell volume as well, and vice versa, so the different intensity threshold used is theoretically likely to result in the same cell abundance. Moreover, although fluctuations might exist, such as fluorescence intensity per cell might change due to physiological changes, threshold setting revision between samples can prevent effects on cell abundance estimation. Thus, reproducible, comparable results with high precision can be obtained using our technique.

The success in all our initial attempts to couple TC-LSFM with several currently available probes indicates that the proposed technique shows potential for applications that reveal the physiological conditions, including cell proliferation, apoptosis, mitosis, and hypoxia stress, from deep inside coral tissue. Among these conditions, a Symbiodiniaceae mitotic index is an important parameter in determining the symbiosis status of coral holobionts (Nielsen et al., 2018; Wilkerson, Kobayashi, & Muscatine, 1988). Conventionally, this index is estimated by counting doublet Symbiodiniaceae cells (Wilkerson,

Parker, & Museatine, 1983), which are actually cytokinetic cells that progress from mitotic cells. In the present study, we demonstrated that immunostaining coupled with TC-LSFM could be applied to accurately estimate the mitotic index. With time-serial sampling, the proposed technique would be instrumental to investigate coral development processes, including metamorphosis of coral larvae and establishment of symbiosis with Symbiodiniaceae, which are critical components of coral population recruitment and growth (James, Smith, Heyward, Baird, & Pratchett, 2013; Lukoschek, Cross, Torda, Zimmerman, & Willis, 2013).

Hypoxia has been suggested to be an underestimated factor responsible for the decline of some coral reefs (Altieri et al., 2017). Although photosynthesis by Symbiodiniaceae creates an oxic or superoxic environment during daytime, ambient water can become hypoxic at night, causing stress in corals (Colombo-Pallotta, Rodríguez-Román, & Iglesias-Prieto, 2010; Dodt et al., 2007; Wooldridge, 2013). Episodic hypoxia events have been recorded during coral spawning events (Simpson, Cary, & Masini, 1993) or phytoplankton blooms (Guzmán, Cortés, Glynn, & Richmond, 1990), eventually causing the extensive mortality of corals and other reef animals in wide areas. Although dissolved oxygen in the gastric cavity of a coral can be measured under laboratory conditions (Agostini et al., 2012), cellular oxygen tension and differential oxygen consumptions by Symbiodiniaceae and by coral hosts have yet to be determined. The gradient of the intracellular hypoxyprobe signal documented here illustrated the diffusion deficiency of oxygen from epidermis to aboral tissue and the respiration of both coral and Symbiodiniaceae cells. With TC-LSFM imaging combined with other techniques, the correlation of cellular hypoxia in coral holobionts with the different genus of Symbiodiniaceae, metabolic condition, apoptosis, and other symptoms of physiological stress could be determined.

TC-LSFM imaging is promising for more studies than shown above. One example is to investigate the distribution and "shuffling" of different genus of Symbiodiniaceae in a coral experiencing thermal or other environmental stress. This technique can be implemented through fluorescence in situ hybridization (FISH) of the sample with a genotype-specific DNA probe, which has been previously coupled with flow cytometry to quantify symbiont assemblages (McIlroy, Smith, & Geller, 2014). The spatial differentiation and temporal dynamics of thermal-sensitive and thermal-resistant genotypes can be monitored in situ and in toto in the course of bleaching and recovery, providing data badly needed to test the debated coral adaptive bleaching hypothesis (Baker, 2001; Hoegh-Guldberg, Jones, Ward, & Loh, 2002). Although some technical challenge remains to be addressed, TC-LSFM coupled with RNA-FISH can be used to profile the cell-specific expression of candidate genes in a whole coral tissue, which is impossible through qPCR (Seneca et al., 2010), transcriptome profiling (Palumbi, Barshis, Traylor-Knowles, & Bay, 2014), or sectioning-coupled RNA-FISH (Traylor-Knowles, Rose, & Palumbi, 2017).

In addition to the enhancement of data depth and accuracy, TC-LSFM can enable the measurement of multiple parameters on one sample, when properly labelled probes are available. For example, information on Symbiodiniaceae density, cell proliferation, and apoptosis can be obtained from one sample as long as specific fluorescence probes are available and can be detected through proper filter arrays. With this multiplex approach, correlation between different biological parameters can be achieved with enhanced consistency and reproducibility. Furthermore, this technique reduces the demand for coral samples in research, thereby making it conservation friendly.

TC-LSFM imaging opens up a new horizon in coral biology, and its power to light up the internal world of corals is potentially revolutionary. Coupled with advances in the development of molecular probes and in genomic data (Bhattacharya et al., 2016; Lin et al., 2015; Shinzato et al., 2011; Shoguchi et al., 2013), the technique can be instrumental for gaining unprecedented depths of understanding on the mechanisms of coral bleaching and resilience under global climate change, and for acquiring information not only of interest to researchers but also fundamental for informed management and conservation of the endangered coral reef ecosystem. Finally, TC-LSFM approach could be adoptable to coral pathology or many other symbiosis cases.

ACKNOWLEDGEMENT

We thank L. Li and W. Yang for their help in underwater sampling and coral aquarium maintenance, respectively. This work was supported by the Natural Science Foundation of China (Grant NSFC 31661143029) and the National Key Research and Development Program of China (Grant 2016YFA0601202 and 2017YFC1404302); the Research Grants Council Collaborative Research Fund of the Hong Kong Special Administrative Region, China (Project 8730037 for SHC); the China Postdoctoral Science Foundation (2017 M620271); and the Outstanding Postdoctoral Scholarship, State Key Laboratory of Marine Environmental Science at Xiamen University (for CL).

CONFLICT OF INTEREST

The authors declare no conflict of interest.

ORCID

Chichi Liu https://orcid.org/0000-0002-5190-2771

REFERENCES

Agostini, S., Suzuki, Y., Higuchi, T., Casareto, B. E., Yoshinaga, K., Nakano, Y., & Fujimura, H. (2012). Biological and chemical characteristics of the coral gastric cavity. *Coral Reefs*, *31*, 147–156. https://doi.org/10.1007/s00338-011-0831-6

Altieri, A. H., Harrison, S. B., Seemann, J., Collin, R., Diaz, R. J., & Knowlton, N. (2017). Tropical dead zones and mass mortalities on coral reefs. *Proceedings of the National Academy of Sciences*, *114*, 3660–3665.

Azaripour, A., Lagerweij, T., Scharfbillig, C., Jadczak, A. E., Willershausen, B., & Van Noorden, C. J. (2016). A survey of clearing techniques for 3D imaging of tissues with special reference to connective. *Progress in Histochemistry and Cytochemistry*, *51*, 9–23. https://doi.org/10.1016/j.proghi.2016.04.001

Baker, A. C. (2001). Reef corals bleach to survive change. *Nature*, *411*, 765–766. https://doi.org/10.1038/35081151

Bhattacharya, D., Agrawal, S., Aranda, M., Baumgarten, S., Belcaid, M., Drake, J. L., … Falkowski, P. G. (2016). Comparative genomics explains

the evolutionary success of reef-forming corals. *eLife*, *5*, e13288. https://doi.org/10.7554/eLife.13288

Capoulade, J., Reynaud, E. G., & Wachsmuth, M. (2013). Imaging marine life with a thin light-sheet. In E. G. Reynaud (Ed.), *Imaging marine life: Macrophotography and microscopy approaches for marine biology* (pp. 186–209). Weinheim, Germany: Wiley-VCH Verlag GmbH & Co. KGaA.

Chung, K., Wallace, J., Kim, S. Y., Kalyanasundaram, S., Andalman, A. S., Davidson, T. J., … Deisseroth, K. (2013). Structural and molecular interrogation of intact biological systems. *Nature*, *497*, 332–337. https://doi.org/10.1038/nature12107

Colombo-Pallotta, M. F., Rodríguez-Román, A., & Iglesias-Prieto, R. (2010). Calcification in bleached and unbleached *Montastraea faveolata*: Evaluating the role of oxygen and glycerol. *Coral Reefs*, *29*, 899–907. https://doi.org/10.1007/s00338-010-0638-x

Davy, S. K., Allemand, D., & Weis, V. M. (2012). Cell biology of cnidarian-dinoflagellate symbiosis. *Microbiology and Molecular Biology Reviews*, *76*, 229–261.

De'ath, G., Fabricius, K. E., Sweatman, H., & Puotinen, M. (2012). The 27-year decline of coral cover on the Great Barrier Reef and its causes. *Proceedings of the National Academy of Sciences*, *109*, 17995–17999.

Dodt, H. U., Leischner, U., Schierloh, A., Jährling, N., Mauch, C. P., Deininger, K., … Becker, K. (2007). Ultramicroscopy: Three-dimensional visualization of neuronal networks in the whole mouse brain. *Nature Methods*, *4*, 331–336. https://doi.org/10.1038/nmeth1036

Guzmán, H. M., Cortés, J., Glynn, P. W., & Richmond, R. H. (1990). Coral mortality associated with dinoflagellate blooms in the Eastern Pacific (Costa Rica and Panama). *Marine Ecology Progress Series*, *60*, 299–303. https://doi.org/10.3354/meps060299

Hoegh-Guldberg, O. (1999). Climate change, coral bleaching and the future of the world's coral reefs. *Marine and Freshwater Research*, *50*, 839–866.

Hoegh-Guldberg, O., Jones, R. J., Ward, S., & Loh, W. K. (2002). Communication arising. Is coral bleaching really adaptive? *Nature*, *415*, 601–602. https://doi.org/10.1038/415601a

Hoegh-Guldberg, O., Mumby, P., Hooten, A. J., Steneck, R. S., Greenfield, P., Gomez, E., … Hatziolos, M. E. (2007). Coral reefs under rapid climate change and ocean acidification. *Science*, *318*, 1737–1742. https://doi.org/10.1126/science.1152509

Hughes, T. P., Anderson, K. D., Connolly, S. R., Heron, S. F., Kerry, J. T., Lough, J. M., … Wilson, S. K. (2018). Spatial and temporal patterns of mass bleaching of corals in the Anthropocene. *Science*, *359*, 80–83. https://doi.org/10.1126/science.aan8048

Hughes, T. P., Baird, A. H., Bellwood, D. R., Card, M., Connolly, S. R., Folke, C., … Roughgarden, J. (2003). Climate change, human impacts, and the resilience of coral reefs. *Science*, *301*, 929–933. https://doi.org/10.1126/science.1085046

Hughes, T. P., Barnes, M. L., Bellwood, D. R., Cinner, J. E., Cumming, G. S., Jackson, J. B. C., … Scheffer, M. (2017). Coral reefs in the Anthropocene. *Nature*, *546*, 82–90. https://doi.org/10.1038/nature22901

Hughes, T. P., Kerry, J. T., Álvarez-Noriega, M., Álvarez-Romero, J. G., Anderson, K. D., Baird, A. H., … Wilson, S. K. (2017). Global warming and recurrent mass bleaching of corals. *Nature*, *543*, 373–377. https://doi.org/10.1038/nature21707

Hughes, T. P., Kerry, J. T., Baird, A. H., Connolly, S. R., Dietzel, A., Eakin, C. M., … Torda, G. (2018). Global warming transforms coral reef assemblages. *Nature*, *556*, 492–496. https://doi.org/10.1038/s41586-018-0041-2

Huisken, J., & Stainier, D. Y. R. (2009). Selective plane illumination microscopy techniques in developmental biology. *Development*, *136*, 1963–1975. https://doi.org/10.1242/dev.022426

Huisken, J., Swoger, J., Del Bene, F., Wittbrodt, J., & Stelzer, E. H. K. (2004). Optical sectioning deep inside live embryos by Selective Plane Illumination Microscopy. *Science*, *305*, 1007–1009.

James, P., Smith, L. D., Heyward, A. J., Baird, A. H., & Pratchett, M. S. (2013). Recovery of an Isolated coral reef system following severe disturbance. *Science*, *340*, 69–71.

Laissue, P. P., Alghamdi, R. A., Tomancak, P., Reynaud, E. G., & Shroff, H. (2017). Assessing phototoxicity in live fluorescence imaging. *Nature Methods*, *14*, 657–661. https://doi.org/10.1038/nmeth.4344

LaJeunesse, T. C., Parkinson, J. E., Gabrielson, P. W., Jeong, H. J., Reimer, J. D., Voolstra, C. R., & Santos, S. R. (2018). Systematic revision of Symbiodiniaceae highlights the antiquity and diversity of coral endosymbionts. *Current Biology*, *28*, 2570–2580. https://doi.org/10.1016/j.cub.2018.07.008

Lin, S., Cheng, S., Song, B., Zhong, X., Lin, X., Li, W., … Morse, D. (2015). The *Symbiodinium kawagutii* genome illuminates dinoflagellate gene expression and coral symbiosis. *Science*, *350*, 691–694. https://doi.org/10.1126/science.aad0408

Lukoschek, V., Cross, P., Torda, G., Zimmerman, R., & Willis, B. L. (2013). The importance of coral larval recruitment for the recovery of reefs impacted by Cyclone Yasi in the Central Great Barrier Reef. *PLoS ONE*, *8*, e65363. https://doi.org/10.1371/journal.pone.0065363

McIlroy, S. E., Smith, G. J., & Geller, J. B. (2014). FISH-Flow: a quantitative molecular approach for describing mixed clade communities of *Symbiodinium*. *Coral Reefs*, *33*, 157–167. https://doi.org/10.1007/s00338-013-1087-0

Mullen, A. D., Treibitz, T., Roberts, P. L., Kelly, E. L., Horwitz, R., Smith, J. E., & Jaffe, J. S. (2016). Underwater microscopy for in situ studies of benthic ecosystems. *Nature Communications*, *7*, 12093. https://doi.org/10.1038/ncomms12093

Nielsen, D. A., Petrou, K., & Gates, R. D. (2018). Coral bleaching from a single cell perspective. *The ISME Journal*, *12*, 1558–1567. https://doi.org/10.1038/s41396-018-0080-6

Palumbi, S. R., Barshis, D. J., Traylor-Knowles, N., & Bay, R. A. (2014). Mechanisms of reef coral resistance to future climate change. *Science*, *344*, 895–898. https://doi.org/10.1126/science.1251336

Power, R. M., & Huisken, J. A. (2017). Guide to light-sheet fluorescence microscopy for multiscale imaging. *Nature Methods*, *14*, 360–373. https://doi.org/10.1038/nmeth.4224

Putnam, H. M., Barott, K. L., Ainsworth, T. D., & Gates, R. D. (2017). The vulnerability and resilience of reef-building corals. *Current Biology*, *27*, R528–R540. https://doi.org/10.1016/j.cub.2017.04.047

Reynaud, E. G., Peychl, J., Huisken, J., & Tomancak, P. (2015). Guide to light-sheet microscopy for adventurous biologists. *Nature Methods*, *12*, 30–34.

Richardson, D. S., & Lichtman, J. W. (2015). Clarifying Tissue Clearing. *Cell*, *162*, 246–257.

Rowan, R., & Knowlton, N. (1995). Intraspecific diversity and ecological zonation in coral-algal symbiosis. *Proceedings of the National Academy of Sciences*, *92*, 2850–2853. https://doi.org/10.1073/pnas.92.7.2850

Seneca, F. O., Forêt, S., Ball, E. E., Smith-Keune, C., Miller, D. J., & van Oppen, M. J. (2010). Patterns of gene expression in a scleractinian coral undergoing natural bleaching. *Marine Biotechnology (New York, N.Y.)*, *12*, 594–604. https://doi.org/10.1007/s10126-009-9247-5

Shapiro, O. H., Kramarsky-Winter, E., Gavish, A. R., Stocker, R., & Vardi, A. A. (2016). Coral-on-a-Chip Microfluidic Platform Enabling Live-Imaging Microscopy of Reef-Building Corals. *Nature Communications*, *7*, 10860.

Shinzato, C., Shoguchi, E., Kawashima, T., Hamada, M., Hisata, K., Tanaka, M., … Satoh, N. (2011). Using the Acropora digitifera genome to understand coral responses to environmental change. *Nature*, *476*, 320–323. https://doi.org/10.1038/nature10249

Shoguchi, E., Shinzato, C., Kawashima, T., Gyoja, F., Mungpakdee, S., Koyanagi, R., … Satoh, N. (2013). Draft assembly of the *Symbiodinium minutum* nuclear genome reveals dinoflagellate gene structure. *Current Biology*, *23*, 1399–1408. https://doi.org/10.1016/j.cub.2013.05.062

Simpson, C. J., Cary, J. L., & Masini, R. J. (1993). Destruction of corals and other reef animals by coral spawn slicks on Ningaloo Reef, Western Australia. *Coral Reefs*, *12*, 185–191. https://doi.org/10.1007/BF00334478

Stat, M., Morris, E., & Gates, R. D. (2008). Functional diversity in coral–dinoflagellate symbiosis. *Proceedings of the National Academy of Sciences*, *105*, 9256–9261.

Traylor-Knowles, N., Rose, N. H., & Palumbi, S. R. (2017). The cell specificity of gene expression in the response to heat stress in corals. *The Journal of Experimental Biology*, *220*, 1837–1845. https://doi.org/10.1242/jeb.155275

van Oppen, M. J. H., & Lough, J. (Eds.) (2008). *Coral bleaching: Patterns, processes, causes and consequences*. Berlin: Springer Verlag.

Weis, V. M. (2008). Cellular mechanisms of Cnidarian bleaching: Stress causes the collapse of symbiosis. *The Journal of Experimental Biology*, *211*, 3059–3066. https://doi.org/10.1242/jeb.009597

Wilkerson, F. P., Kobayashi, D., & Muscatine, L. (1988). Mitotic index and size of symbiotic algae in Caribbean Reef corals. *Coral Reefs*, *7*, 29–36.

Wilkerson, F. P., Parker, G. T., & Museatine, L. (1983). Temporal patterns of cell division in natural populations of endosymbiotic algae. *Limnology and Oceanography*, *28*, 1009–1014.

Wooldridge, S. (2013). A new conceptual model of coral biomineralisation: hypoxia as the physiological driver of skeletal extension. *Biogeosciences*, *10*, 2867–2884. https://doi.org/10.5194/bg-10-2867-2013

Yang, B., Treweek, J.B., Kulkarni, R.P., Deverman, B.E., Chen, C.K., Lubeck, E., Shah, S., Cai, L., & Gradinaru, V. (2014). Single-Cell Phenotyping within Transparent Intact Tissue through Whole-Body Clearing. *Cell*, *158*, 945–958. https://doi.org/10.1016/j.cell.2014.07.017

Zoccola, D., Morain, J., Pagès, G., Caminiti-Segonds, N., Giuliano, S., Tambutté, S., & Allemand, D. (2017). Structural and functional analysis of coral hypoxia inducible factor. *PLoS ONE*, *12*, e0186262. https://doi.org/10.1371/journal.pone.0186262

SUPPORTING INFORMATION

Additional supporting information may be found online in the Supporting Information section at the end of the article.

How to cite this article: Liu C, Cheng SH, Lin S. Illuminating the dark depths inside coral. *Cellular Microbiology*. 2020; 22:e13122. https://doi.org/10.1111/cmi.13122